crystals

MDPI

Article

Research on Secondary Recrystallization Mechanism of Oriented Silicon Steel

Xuming Liu [1,2,*], Qiwu Jiang [3], Yitong Wang [1,2], Haili Zhang [4], Zhiwei Jia [4], Xianglong Wang [4], Xiaoda Wang [3], Qinglei You [3], Zhiping Hu [1,4,*], Jinsong Meng [3] and Yidong Wang [3]

1 Key Laboratory of Metal Material for Marine Equipment and Application, 63 Wuyi Road, Anshan 114009, China; agbjywyt@163.com
2 Ansteel Beijing Research Institute Co., Ltd., Beijing 102211, China
3 Angang Steel Co., Ltd., Anshan 114021, China; jiangqiwu@ansteel.com.cn (Q.J.); wangxiaoda@ansteel.com.cn (X.W.); youqinglei@ansteel.com.cn (Q.Y.); mengjinsong@ansteel.com.cn (J.M.); wangyidong@ansteel.com.cn (Y.W.)
4 Ansteel Iron & Steel Research Institutes, Anshan 114009, China; zhanghaili@ansteel.com.cn (H.Z.); jiazhiwei@ansteel.com.cn (Z.J.); wangxianglong@ansteel.com.cn (X.W.)
* Correspondence: 15832555952@163.com (X.L.); huzhiping900401@126.com (Z.H.)

Abstract: Based on the understanding that the essence of secondary recrystallization of Goss texture is to restrain the abnormal growth of {110}<112>, {210}<001> and partial Goss texture {110}<225>, it was concluded that making sharp Goss grow up becomes the only choice. It was proposed that the abnormal growth mechanism of Goss texture was the result of selective generation, directed inheritance, and selective growth. The mechanism explained that the Goss texture was the most easily formed shear texture. In directed inheritance, the Goss texture was required to be highly compatible with the near-constant of the second-phase particle inhibition force, providing an optimal environment for the abnormal growth of the Goss texture by controlling the inhibition force near-constant. The control of the near-constant inhibition force provides an optimal environment for the abnormal growth of the Goss texture. Based on that, the process technology for producing low-temperature nitrided-oriented silicon steels and steel products was successfully developed.

Keywords: oriented silicon steel; secondary recrystallization mechanism; inhibition force near constant; selective generation; directed inheritance; selective growth

Citation: Liu, X.; Jiang, Q.; Wang, Y.; Zhang, H.; Jia, Z.; Wang, X.; Wang, X.; You, Q.; Hu, Z.; Meng, J.; et al. Research on Secondary Recrystallization Mechanism of Oriented Silicon Steel. *Crystals* **2023**, *13*, 1396. https://doi.org/10.3390/cryst13091396

Academic Editor: José L. García

Received: 22 August 2023
Revised: 15 September 2023
Accepted: 18 September 2023
Published: 19 September 2023

1. Introduction

The oriented silicon steel is a kind of soft magnetic material used to manufacture transformers and large generators, and it has a sharp Goss texture {110}<001> and a great insulating surface [1–4]. The mechanism of secondary recrystallization has not been known for about 70 years since the discovery of the abnormal growth of Goss [5]. Recently, the mechanisms of abnormal growth have been widely studied, such as the size dominance mechanism [6], the aggregation nucleation theory [7], and the solid-state wetting theory [8]. Nevertheless, the above theories have either been disproved or not verified by experiments [9–11]. The theories with high acceptance are the high energy (HE) grain boundaries (GB) theory [12,13] and the coincidence site lattice (CSL) theory [14], which explain the secondary recrystallization of Goss texture from the grain boundary and crystal structure perspectives. However, the main point in common between the two theories is that some special GB types are easily formed around Goss grains (such as $\sum$3–9 in the CSL model and 15–45° disorientation in the HE model), and the particles can easily dissolve at those particular types of GBs, resulting in a strain or even a disappearance of the pinning effect [15]. Northeastern University describes the kinetic process of secondary recrystallization of oriented silicon steel utilizing grain boundary energy [16] and concludes that orientation selection behavior results from the multi-factor coupling. The above studies

have not yet clarified the role of the second-phase particle inhibition force in the unique growth of Goss.

In this paper, the hereditary characteristics of Goss texture and growth environment were studied, and the abnormal growth of Goss texture in oriented silicon steel was revealed to be the result of different effects of inhibition force, grain boundary energy, surface energy, and other factors at the early, middle, and end of high-temperature annealing. The optimal environment for the abnormal growth of Goss texture results from the accurate control of the whole process, such as hot working, cold working, and additional inhibitors.

2. Materials and Methods

2.1. Process Flow of Low-Temperature Nitrided-Oriented Silicon Steel

The study on the mechanism of abnormal growth of Goss texture is based on the production process of oriented silicon steel with low-temperature slab heating combined with nitriding (Figure 1a): melted iron→Converter smelting→vacuum refining→continuous casting→hot rolling→normalizing→cold rolling→decarburization+nitriding+coating MgO→high temperature annealing→hot drawing annealing→recoiling→finished product. Industrial Fe-3%Si steel was used as the raw material in this study (Table 1). The hot-rolled temperature was 1200 °C, and the time was about 200 min. The normalized process was divided into two parts: first, 1100 °C for 20 s, then 900 °C for 120 s. The cold rolling was adopted by 6 passes, with a total strain of more than 88%. As for the decarburization, the low-temperature nitriding was adopted at 850 °C for 120 s, and the high-temperature nitriding was treated at 950 °C for 20 s. In the high-temperature annealing, the steel was treated at 1200 °C for 30 h. At last, the steel was hot-drawing annealed at 880 °C for 20 s. The microstructure of hot-rolled steel is shown in Figure 1b.

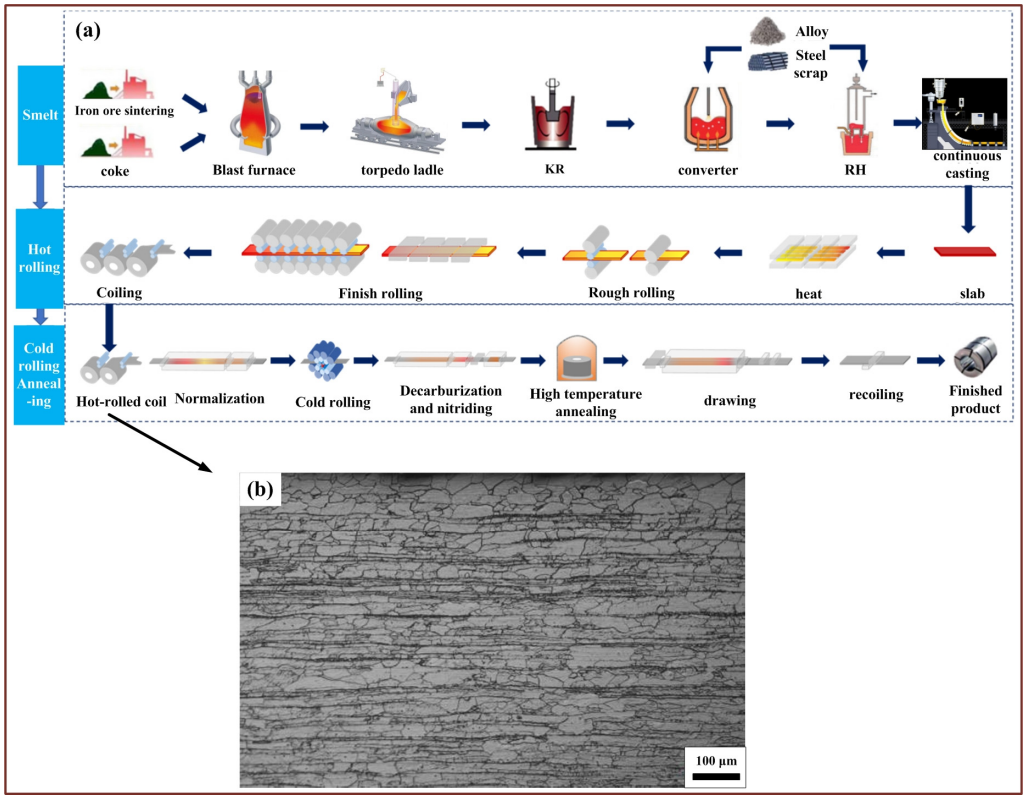

Figure 1. Production process flow of low-temperature nitrided-oriented silicon steel (**a**) and the microstructure of hot-rolled steel (**b**).

Table 1. The chemical composition of oriented silicon steel (wt.%).

C	Si	Mn	P	S	N	Als	Fe
0.04–0.056	2.9–3.2	0.1–0.2	0.01–0.013	0.005–0.007	0.006–0.008	0.01–0.02	Bal.

2.2. Characterizations

In this study, the micro-texture was tested by EBSD (Electron Back Scattered Diffraction) (Carl Zeiss AG, Oberkochen, Germany) on a GeminiSEM 300 scanning electron microscope under a voltage of 20 KV, and the data was analyzed by HKL Channel 5 software. The macro-texture was tested by a Brucker D8 Advance X-ray diffractometer (XRD) (Brucker, Saarbrucken, Germany). The pole figures of (110), (200), and (211) were measured to calculate the ODF (orientation distribution function) figure.

3. Results

The Goss grain originates from hot rolling, after normalizing, cold rolling, and primary recrystallization. The abnormal growth occurs during high-temperature annealing. Understanding the texture transformation rules of hot deformation, cold deformation, and primary recrystallization is the premise for revealing the abnormal growth mechanism of Goss texture during high-temperature annealing.

3.1. The Origination of Goss Texture

After smelting and refining, the hot billet was sent to the hot rolling furnace. After the maximum homogenization heat treatment of austenite, the grains were broken by rapid rough rolling with a high strain rate, and the high deformation rate of finish rolling formed the Goss texture. Ferrite becomes supersaturated with respect to AlN after quenching and high-temperature coiling after high-temperature finishing rolling.

Figure 2 shows the texture type of oriented silicon steel during hot rolling. It is shown that in the surface layer of the hot-rolled plate, the cubic and γ fiber textures appear. In the sub-surface are three kinds of shear textures, i.e., Goss {110}, copper {112}, and brass {110}; in the middle layer are strong rotated cubic {100}<011> and weak {111}<112> textures.

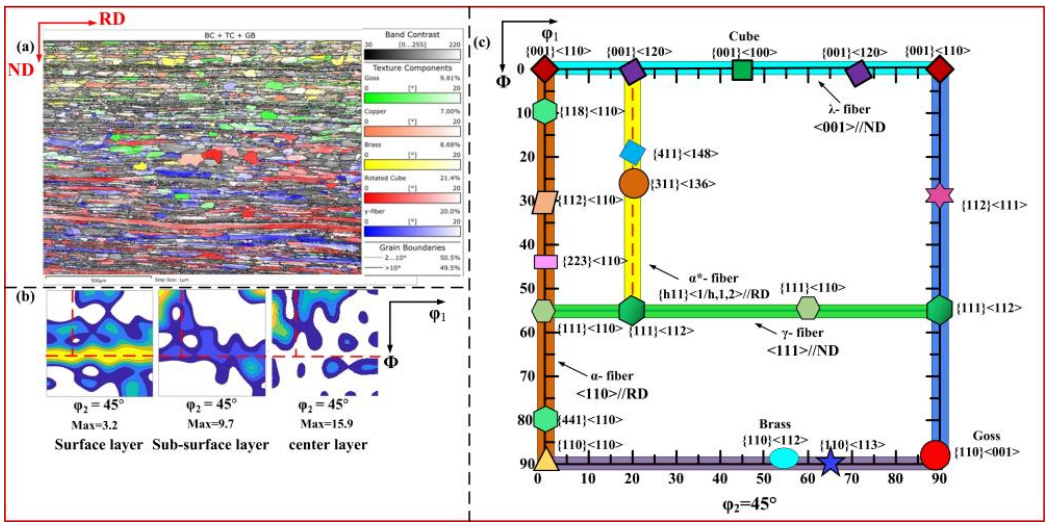

Figure 2. Texture type of hot-rolled-oriented silicon steel. (**a**) XRD ODF Φ_2 = 45° cross-section; (**b**) EBSD orientation image; (**c**) important orientation in the BCC (body-centered cubic). (ND-normal direction, RD-rolling direction, BC-band contrast, TC-texture component, GB-grain boundary).

As is known, friction shear deformation between the surface of the hot-rolled plate and the roller results in grain slip and rotation. Thus, three kinds of shear textures are formed: the Goss texture is first formed, then the brass texture, and the copper texture at last [17]. The initial orientation of the Goss texture is cube texture, and the initial orientation of the

brass texture is 25° to the rotating cube. As for the copper texture, the initial orientation belongs to the rotating cube.

To sum up, the Goss texture of oriented silicon steels is made by the shear deformation of hot-rolled cube texture, which is made under specific process conditions. The origin of the secondary recrystallization of Goss texture is described by referring to "selective nucleation" in the theory of primary recrystallization and modifying it to "selective generation".

3.2. The Hereditary Characteristics of Goss Texture before Secondary Recrystallization

3.2.1. In Situ Inheritance of Goss Texture after Normalizing

The normalization process of low-temperature nitrided-oriented silicon steel was a critical process that ensured the homogenization of the cold deformation structure and the formation of AlN precipitates. The supersaturated Al and N elements in the matrix were precipitated by a two-stage normalization process, and the designed AlN precipitate size and distribution density were obtained. The texture type of normalized-oriented silicon steels is shown in Figure 3.

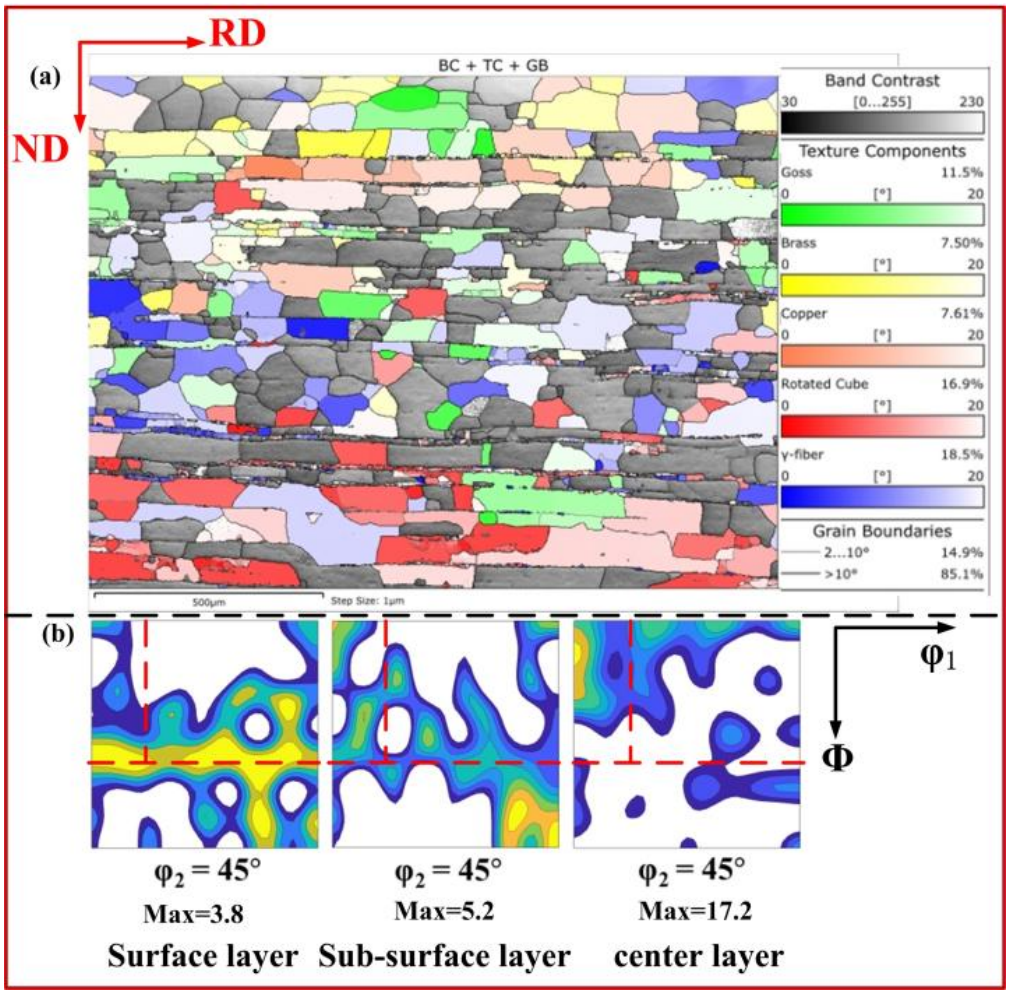

Figure 3. Texture type of normalized-oriented silicon steel. (**a**) XRD ODF Φ_2 = 45° cross-section; (**b**) EBSD orientation image.

As is seen in Figure 3, the texture type of the hot-rolled plate remains unchanged after normalizing, and the Goss texture is inherited in situ by normalizing; {110}<001> and {100}<011> are strengthened, while {111}<112> is weakened. The brass texture and the copper texture are enhanced slightly.

3.2.2. The Goss Texture Orientation Changes after Cold Deformation

In the cold rolling process, a high strain of more than 35% was used at the first three passes. At the third pass, aging rolling was used; the last two passes were used to control the plate shape, and the total strain was more than 88%. Many transitional zones were formed after rolling. Figure 4 shows the texture type after cold rolling. As is shown, after cold rolling, the α texture mainly as {001}<110>, {112}<110> and γ texture mainly as {111}<110>, {111}<112> have appeared; the ferrite {112}<110> transformed to {411}<148>. After severe deformation, there is a transformation relationship between {411}<148> and {112}<110>.

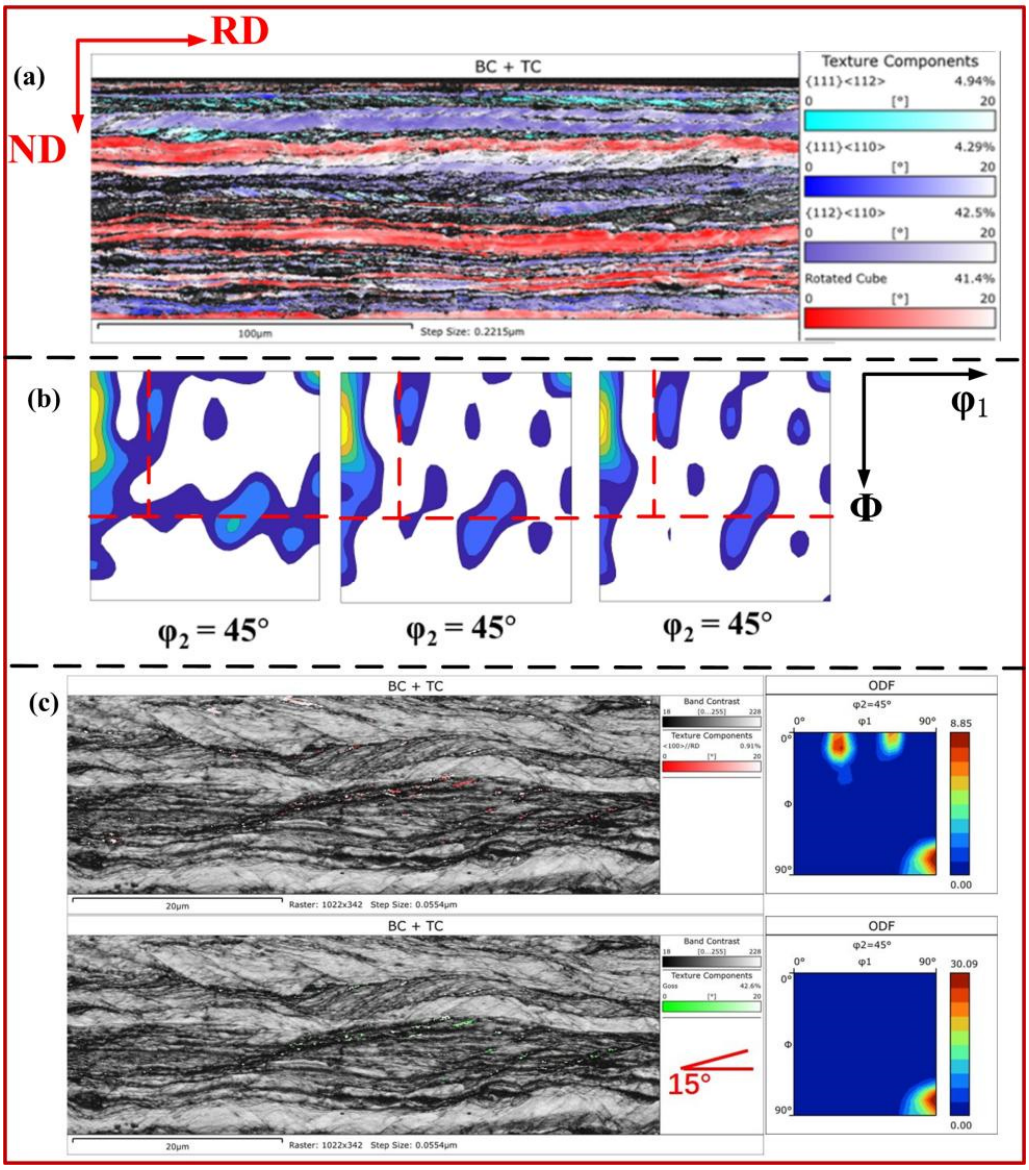

Figure 4. Texture type of cold-rolled-oriented silicon steel. (**a**) XRD ODF Φ_2 = 45° cross-section; (**b**) EBSD orientation image; (**c**) Goss sub-grain in the two {111}<112> shear zones.

The normalized Goss texture mostly transformed to {111}<112> after rolling deformation; a small part is left upon the transition zone between the two {111}<112> shear zones, and it remains the in situ oriented Goss sub-grains (Figure 4).

3.2.3. The Goss Texture Orientation Changed in Primary Recrystallization

Figure 5 shows the primary recrystallization texture type. As shown in Figure 5, the surface and sub-surface layers are mainly {411}<148>, {111}<112>, and a few Goss textures,

while the middle layer is {411}<148>, {111}<112>, and {001}<210>. A small amount of {111}<112> remains after cold rolling, transformed into Goss after primary recrystallization. In the transition zone, the Goss orientation grows in situ.

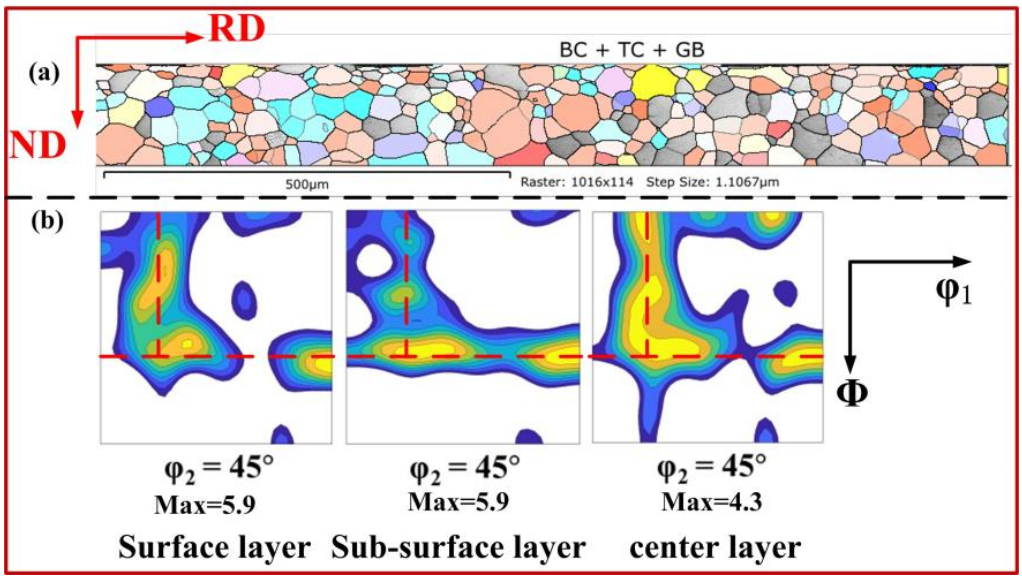

Figure 5. Primary recrystallization texture type of oriented silicon steel. (**a**) XRD ODF Φ_2 = 45° cross-section; (**b**) EBSD orientation image.

4. Discussion

4.1. Directed Inheritance Behavior of Goss Texture before Secondary Recrystallization

The distribution of texture for hot rolling, cold rolling, and primary recrystallization in the ODF constant Φ_2 = 45° cross-section diagram is shown in Figure 6. It shows that, after cold rolling, the originated hot-rolled Goss texture transformed into {111}<112>, Goss, and the texture types after primary recrystallization, elucidating the directional genetic characteristics of Goss. The "directed growth" in the primary recrystallization theory was displaced to "directed inheritance" to describe the orientation transformation behavior of the Goss texture before secondary recrystallization.

4.2. The Preferred Environment for Goss to Grow Up Abnormally

The essence of secondary recrystallization of Goss texture is to inhibit the abnormal growth of {110}<112>, {210}<001>, and partial Goss texture {110}<225>, so that sharp Goss growth is the only choice.

In order to provide the perfect environment for sharp Goss to grow up abnormally, it should satisfy several conditions: Firstly, the precise setting of the harsh ranges Al and N makes the total amount of congenital inhibitors nearly constant. Secondly, the process design of hot rolling and cold rolling achieves nearly constant innate inhibition force. Thirdly, Al and the remaining free Al after binding with innate N combine with acquired infiltration N to achieve a near-constant amount of acquired inhibitor.

According to the dynamical equation of homogeneous nucleation of AlN [18]:

$$lg\frac{t_{0.05a}}{t_{0a}} = \frac{2}{3}(-1.28994 - 2\lg d * + \frac{\Delta G^* + \frac{5}{2}Q}{\ln 10 \cdot k \cdot T}) \quad (1)$$

where d* is the critical nucleation size of AlN, Q is the diffusion activation energy of AlN, k is boltzmann constant, T is temperature, $t_{0.05a,d,g}$ is nucleation starting time (considering 5% nucleation as starting), $t_{0a,d,g}$ is the effective nucleation time, and ΔG* is the critical

nucleation energy. And the dynamical equation of AlN nucleation at dislocation can be described as [18]:

$$lg\frac{t_{0.05d}}{t_{0d}} = -1.28994 - 2\mathrm{lgd} * + \frac{\Delta G_d{}^* + \frac{5}{3}Q}{\ln 10 \cdot k \cdot T} \quad (2)$$

The dynamical equation for grain boundary nucleation of AlN can be described as [18]:

$$lg\frac{t_{0.05g}}{t_{0g}} = 2(-1.28994 - 2\mathrm{lgd} * + \frac{A_1\Delta G_g{}^* + Q}{\ln 10 \cdot k \cdot T}) \quad (3)$$

We can describe the controlling of inhibitor more quantitatively.

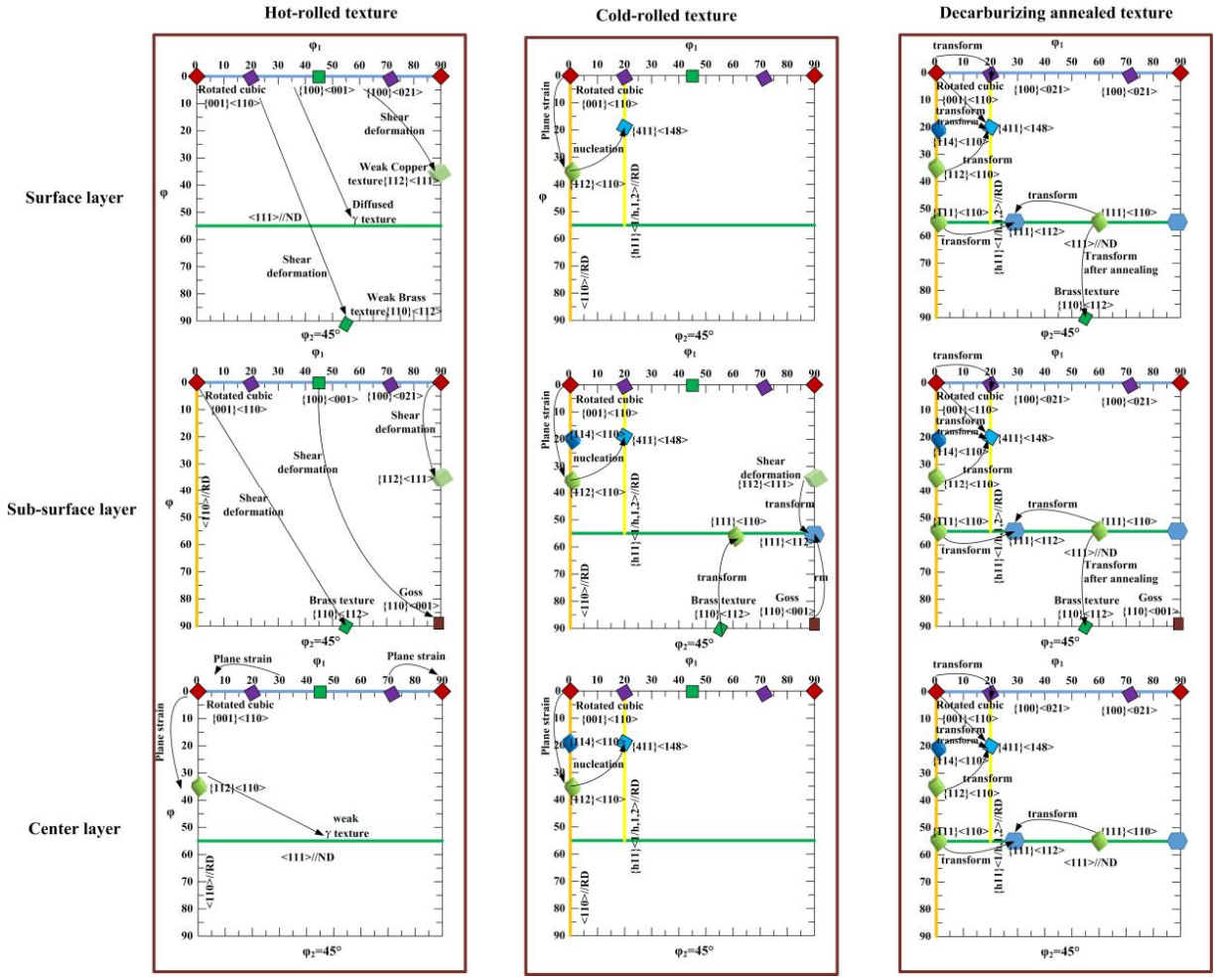

Figure 6. Distribution of Goss texture in hot-rolled-, cold-rolled-, and primary-recrystallized-oriented silicon steel in ODF cross-section of Φ_2 = 45°.

4.2.1. Control Principle of Near-Constant Inhibition of Innate Inhibitor AlN

AlN's quantity and particle size in the billet's core were higher than on the side. Some of them were dissolute at the hot rolling, the size of some of them was reduced, and the coarse rolling with huge strain ensured the structure was uniform. Since finish rolling is quite quick, AlN cannot manage to precipitate from the matrix phase. So the solid solution remains supersaturated. After normalization, the size of AlN-precipitated particles in the surface layer first increased and then decreased with the increase in normalization temperature. The precipitated particles in the middle layer increased as the temperature rose. Due to the enough driving force, the AlN-precipitated particles in the surface layer grow first, but when the temperature is too high to inhibit the growth of AlN, the size of AlN then decreases. Because of the limited time of normalization and the loss of heat

transfer, the precipitated particles in the middle layer were fit for the growth temperature. Controlling the normalization temperature can help the second-phase particles achieve the size distribution as designed. Figure 7 shows the schematic diagram of the changed structure and second phase particles in the continuous casting billet, the heated casting billet, the hot-rolled plate, and the normalized plate.

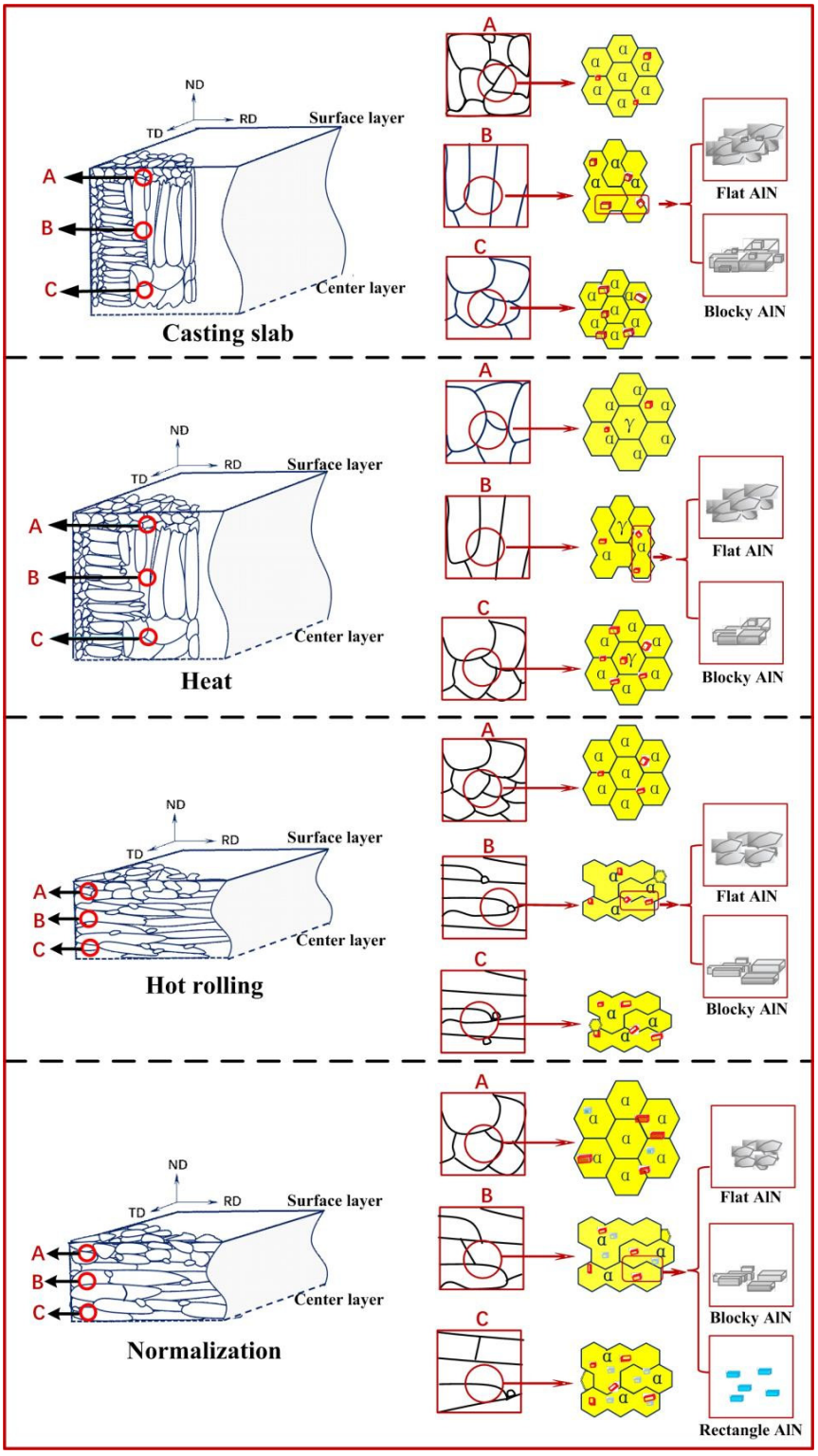

Figure 7. Variation schematic diagrams of microstructures in continuous casting billets, casting billets after hot rolling, hot-rolled steel sheets, and normalized sheets and second phase.

The size of AlN in the normalized plate becomes coarse. The cold-rolled slip dislocation will stop sliding on a coarse AlN surface, and dislocation pile-up and huge stress concentrations are generated, which make AlN rotate randomly relative to the matrix. When their slip system is almost parallel, the dislocation in the matrix can be slid into AlN easily, refining AlN. The refining effect becomes more significant with the increase in cold rolling strain. Meanwhile, the size and distribution of AlN in the cold-rolled plate are nearly uniform [19]. The schematic diagram of cold-deformation AlN cut by dislocation can be seen in Figure 8. Considering Equations (1)–(3), at first, the nucleation of AlN is almost homogeneous; the nucleation process of AlN is based on uniform nucleation and grain boundary nucleation. As the temperature rises, the grain becomes coarser, the location of grain boundary nucleation is limited, and the quick cooling process enhances dislocation density in the matrix so that AlN will precipitate on the dislocation line. The effect of grain boundary nucleation and uniform nucleation becomes weaker, and the dislocation nucleation plays an important role. Based on the above equation and the near-constant theory, we can control the inhibitor more quantitatively.

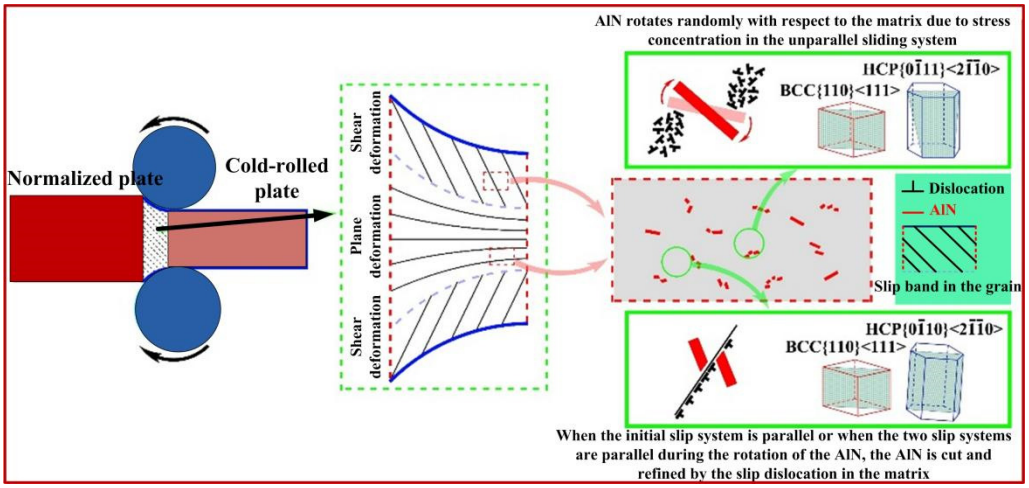

Figure 8. Schematic diagram of cold deformation AlN of oriented silicon steel cut by dislocation.

4.2.2. The Control Principle of Near-Constant Inhibition of Acquired Inhibitor AlN

The acquired inhibitor AlN of oriented silicon steel is produced by infiltration of NH_3 in the decarburization annealing process. Before nitriding, firstly, decarburization must be completed to ensure that the matrix is a single ferrite in the process from low temperature to high temperature during nitriding, which not only ensures the stability of nitriding quality but also ensures the stable growing environment for the second growth of Goss; secondly, we must complete primary recrystallization so that there is appropriate grain size by the efforts of the innate and acquired inhibitions to make sure that Goss grains have the only advantage of growing up.

The nitride types [20] formed by low-temperature nitriding and high-temperature nitriding in the decarburization annealing process are shown in Figure 9. The types of nitrides formed and their distribution in the thickness direction of steel plate are different under low-temperature and high-temperature nitriding conditions. Si_3N_4 has a high content in the low-temperature nitriding (in light color in Figure 9a), and in the surface layer and 1/4 layer, the content of Si_3N_4 is even more than that of AlN, while AlN has a high content in the high-temperature nitriding (in bright color). Low-temperature + high-temperature two-stage nitriding is used to maximally control the AlN of the surface layer, 1/4 layer, and center layer, which remain near-constant. As for the control key points of the AlN precipitates, firstly, as for the structure and thickness of the oxide layer, the pressure and concentration of NH_3 in the infiltrating medium should be controlled to ensure that the infiltration of N is nearly constant. Secondly, ensure that the free aluminum bound with the content of N is in a narrow range so that the AlN generated is almost constant; the

primary conditions for the near-constant control of the inhibition force are created for the high-temperature annealing process. Based on the dynamic nucleation Equations (1)–(3) and the control of the two-stage nitriding process, the near-constant control of innate and acquired inhibitor AlN could be achieved.

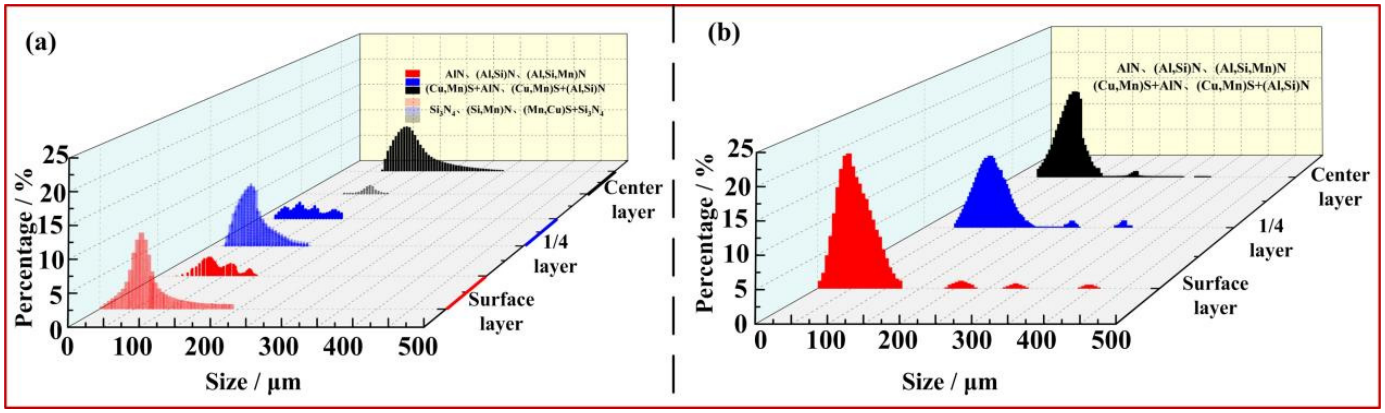

Figure 9. Type of nitride formed during the decarburization annealing process. (**a**) low-temperature nitriding; (**b**) high-temperature nitriding.

4.3. The Mechanism of Goss Texture Abnormal Growth

Goss texture forming at abnormal growth results from the comprehensive action of various driving forces. The growth environment for Goss texture forming at abnormal growth is defined as the "preferential growth" in the primary recrystallization theory, and its connotation is as follows:

Based on the research of Hillert and Ushigami [21], the secondary recrystallization grain growth velocity can be described in the equation below, considering the effect of grain size, grain orientation, and inhibitor [21]:

$$v = \frac{dR_1}{dt} = \alpha m \gamma_m \left(\frac{1}{R_2} - \frac{e}{R_1} - \frac{eZ}{\alpha}\right) \quad (4)$$

where R_1 is the radius of the secondary recrystallization grain, t is secondary recrystallization time, α is the geometric factor, m is grain boundary mobility, γ_m is the grain boundary energy of the matrix, R_2 is the radius of the matrix grains, and e is the relative grain boundary energy coefficient, which can be considered as:

$$e = \gamma_g / \gamma_m \quad (5)$$

where γ_g is the grain boundary energy between secondary recrystallization grains and matrix grains.

Zener established the relationship between the inhibitor pinning force and precipitate volume fraction and radius [22]:

$$Z = 3\frac{f\sigma}{4r} \quad (6)$$

where σ is the interface energy between the precipitates and matrix, f is the volume fraction of precipitates, and r is the mean radius of precipitates.

Based on Equations (4)–(6), we can summarize that:

$$v = \alpha m \gamma_m \left(\frac{1}{R_2} - \frac{\gamma_g}{\gamma_m R_1} - \frac{3\gamma_g f\sigma}{4\gamma_m \alpha r}\right) \quad (7)$$

4.3.1. Role of the Pinning Force at the Initial Stage of Secondary Recrystallization

At the initial stage of secondary recrystallization, the grain of primary recrystallization continues to grow. In this period, Goss grains have no obvious growth advantage, so

they have no size advantage. With the distribution of the actual inhibitor (surface > core layer > 1/4 layer) and the density of second-phase precipitates in differently oriented grains (brass > Goss > copper > {100}<001>) [23], temperature is used to control the content of effective inhibitor precisely, forming different inhibition abilities. In this way, brass {110}<112>, {210}<001> and partial Goss texture {110}<225> were maximally inhibited, while {110}<112>, {114}<841> was slightly inhibited. The precise control of temperature is crucial. When the temperature is high, the inhibitor is too fast to lose its effect, so the inhibitor capability is insufficient and cannot inhibit brass orientation efficiently. When the temperature is too low, the inhibitor capability is too large, so all grains are pinned, and Goss cannot grow in the second period. Based on Equation (7), at the initial stage of secondary recrystallization, the temperature influences the radius and volume fraction of inhibitors, so the grain growth velocity will be influenced, so the pinning force plays a decisive role in this period.

4.3.2. Role of the Grain Boundary Energy at the Middle Stage of Secondary Recrystallization

At the middle stage of secondary recrystallization, the annealing temperature enhanced and the inhibitor capability weakened so that the other grains were unable to swallow Goss. The Goss grains with low grain boundary energy, which can preferentially get rid of precipitate pinning, began to incorporate {411}<148> and {111}<112>, which have a Σ9 grain boundary relationship with the Goss rotation around <110> at about 38.94°. The growth rate of Goss is faster than that of other-oriented grains, such as brass, with a more significant size advantage. As the inhibitor capability distribution is significant in the surface layer and weak in the center layer, the forced Goss texture grows from the sub-surface layer to the center layer. When the subsurface Goss grains grow to the central layer, they will encounter more {411}<148> and {111}<112> oriented grains and proliferate, thus occupying the size advantage of abnormal growth [24]. Based on Equation (7), at the middle stage of secondary recrystallization, when the grains of favorable texture such as {411}<148> and {111}<112> generate, γ_g increases, which will make e < 1, but the Σ9 grain boundary relationship with the Goss rotation around <110> at about 38.94° makes e increase from 0.5 to 0.7, still less than 1, so that will provide more driving force in the middle stage. Thus, in this period, grain boundary energy plays a decisive role.

4.3.3. Role of the Interface Energy at the Later Stage of Secondary Recrystallization

As the annealing temperature rises, the surface contact with H_2 directly increases and the decomposition of the particles in the surface layer will be faster than that of the center layer. The inhibitor capability in the surface layer will be weakened because the {110} plane is the most densely packed plane, which has the lowest interface energy (the surface energy relation of the low exponential surfaces is {110}<{100}<{111}) [25]. After the Goss grain growth, which has been in a dominant position, touches the surface, the low surface energy of the {110} crystal plane can continue to provide the driving force for abnormal growth and promote the further growth of the Goss grain. The brass and Goss orientations both belong to the {110} plane texture, so the surface energy in the H_2 atmosphere has the apparent advantage. If they grow abnormally on the surface and through the plate thickness, it will deteriorate the finished product's properties and should be effectively controlled. Based on Equation (7), at the later stage of secondary recrystallization, when σ is decreased, the grain growth velocity will increase, providing the driving force for Goss grain. So in this period, interface energy plays an important role. The schematic of the abnormal growth of Goss texture in the secondary recrystallization is shown in Figure 10.

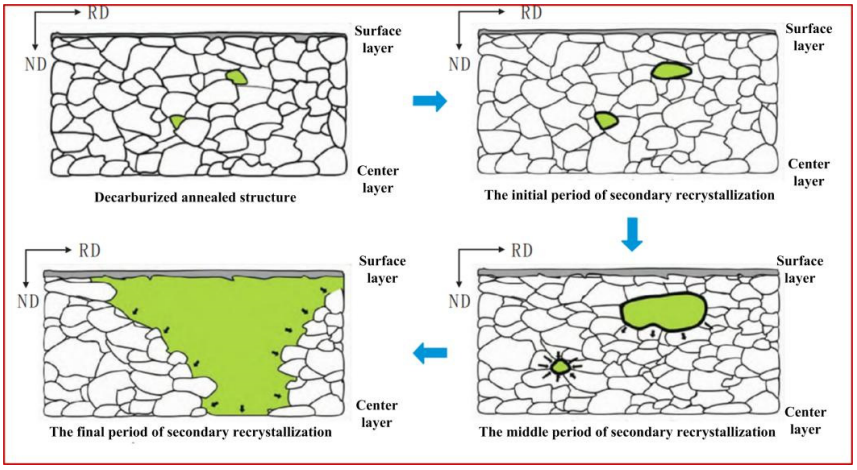

Figure 10. Schematic diagram of abnormal growth of Goss texture secondary recrystallization.

5. Conclusions

In this paper, the process of secondary recrystallization in the oriented steel was explained, and the origin, heredity, and growth mechanism of the Goss texture in the oriented steel were discussed.

(1) The origin of Goss texture is "selective formation" under hot shear deformation conditions.

(2) During the normalizing, cold deformation, and primary recrystallization processes, Goss exhibits a fixed orientation and the characteristic of "directed inheritance".

(3) Goss texture forming at abnormal growth achieves "optimal growth", resulting from the comprehensive action of various driving forces.

Author Contributions: Conceptualization, Q.J.; methodology, visualization, and writing-original draft preparation, X.L. and Y.W. (Yitong Wang); resources, H.Z., X.W. (Xiaoda Wang), X.W. (Xianglong Wang) and Q.Y.; supervision, J.M. and Y.W. (Yidong Wang); writing-review and editing, Z.H. and Z.J. All authors have read and agreed to the published version of the manuscript.

Funding: This research was funded by the National Natural Science Foundation of Liaoning Province, China [Grant No. 2022-MS-450].

Data Availability Statement: Not applicable.

Conflicts of Interest: The authors declare no conflict of interest.

References

1. Matsuo, M. Texture control in the production of grain oriented silicon steels. *ISIJ Int.* **1989**, *29*, 809–827. [CrossRef]
2. Xia, Z.S.; Kang, Y.L.; Wang, Q.L. Developments in the production of grain-oriented electrical steel. *J. Magn. Magn. Mater.* **2008**, *320*, 3229–3233. [CrossRef]
3. Vratislav, S.; Dlouhá, M.; Kalvoda, L. Neutron diffraction texture analysis of grain-oriented steel sheets. *Solid State Phenom.* **2005**, *105*, 175–180. [CrossRef]
4. Yasuyuki, H. Mechanism of secondary recrystallization of Goss grains in grain-oriented electrical steel. *Sci. Technol. Adv. Mater.* **2017**, *18*, 480–497.
5. GOSS, N.P. Electrical Sheet and Method and Apparatus for Its Manufacture and Test. U.S. Patent 1965559, 3 July 1934.
6. May, J.E.; Turnbull, D. Secondary recrystallization in silicon iron. *Trans. Metall. Soc. AIME* **1958**, *212*, 769–781.
7. Inokuti, Y.; Maeda, C.; Ito, Y. Computer color mapping of configuration of Goss grains after transverse cold rolling in grain oriented silicon steel. *Trans. Iron Steel Inst. Jpn.* **2006**, *27*, 302–311. [CrossRef]
8. Hwang, N.M.; Lee, B.J.; Han, C.H. Texture evolution by grain growth under a system of anisotropic grain boundary energy. *Scripta Mater.* **1997**, *37*, 1761–1767. [CrossRef]
9. Chen, N.; Zaefferer, S.; Lahn, L.; Günther, K.; Raabe, D. Effects of topology on abnormal grain growth in silicon steel. *Acta Mater.* **2003**, *51*, 1755–1765. [CrossRef]
10. Lücke, K.; Brandt, R.; Abbruzzese, G. Normal and abnormal grain growth as transient phenomena. *Interface Sci.* **1998**, *6*, 67–76. [CrossRef]

11. Thompson, C.V.; Frost, H.J.; Spaepen, F. The relative rates of secondary and normal grain growth. *Acta Metall.* **1987**, *35*, 887–890. [CrossRef]
12. Hayakawa, Y.; Szpunar, J.A.; Palumbo, G.; Lin, P. The role of grain boundary character distribution in Goss texture development in electrical steels. *J. Magn. Magn. Mater.* **1996**, *160*, 143–144. [CrossRef]
13. Hayakawa, Y.; Szpunar, J.A. The role of grain boundary character distribution in secondary recrystallization of electrical steels. *Acta Mater.* **1997**, *45*, 1285–1295. [CrossRef]
14. Harase, J.; Shimizu, R. Distribution of {110)<001>oriented grains in the primary recrystallized 3% Si-Fe alloy. *Trans. Jpn. Inst. Met.* **1988**, *29*, 388–398.
15. Wang, M.; Xu, Y.; Hu, J.; Fang, F.; Jin, J.; Jia, T.; Peng, Q. Phase-Field Simulation on the Effect of Second-Phase Particles on Abnormal Growth of Goss Grains in Fe-3%Si Steels. *Nanomaterials* **2022**, *12*, 4148. [CrossRef] [PubMed]
16. Xu, Z.Y.; Sha, Y.H.; Zhang, F.; Zhang, H.B.; Li, B.G.; Chu, S.J.; Zuo, L. Orientation selection behavior during secondary recrystallization in grain-oriented silicon steel. *Acta Metall Sin.* **2020**, *56*, 1067–1074.
17. Yan, M.Q.; Qian, H.; Yang, P.; Song, H.J. Behaviors of brass texture and its influence on Goss texture in grain oriented electrical steel. *Acta Metall Sin.* **2012**, *48*, 16–22. [CrossRef]
18. Liu, L.; Qiao, J.L.; Yin, S.B.; Hu, J.W.; Xiang, L.; Qiu, S.T. Kinetics of precipitation for AlN in austenite of grain-oriented silicon steel. *Iron Steel Vanadium Titanium.* **2020**, *41*, 158–162.
19. Wang, X.L.; Zhang, W.N.; Hao, Y.S.; Jiang, Q.W.; Li, D.G.; Li, Y.H.; Li, L. Refinement of coarse AlN by the shear effect of dislocation slip during cold rolling in low-temperature grain-oriented silicon steel. *Intermetallics* **2021**, *132*, 107136. [CrossRef]
20. Cicalé, S. Process for the Production of Grain Oriented Electrical Steel Sheet with High Magnetic Characteristics. E. P. Patent 0950119B1, 2 July 1998.
21. Xu, Z.Y.; Sha, Y.H.; He, Z.H.; Zhang, F.; Liu, W.; Zhang, H.B.; Zuo, L. Complete Goss secondary recrystallization by control of the grain size and texture of primary recrystallization in grain-oriented silicon steel. *Materials* **2021**, *14*, 5383. [CrossRef]
22. Zener, C. Grains, phase, and interfaces: An interpretation of microstructure. *Trans. Am. Inst. Min. Metall. Soc.* **1948**, *175*, 15–51.
23. Jiang, W.N.; Wu, X.L.; Yang, P.; Gu, X.F.; Xie, Q.G. Formation of dynamic recrystallization zone and characteristics of shear texture in surface layer of hot-rolled silicon steel. *Acta Metall. Sin.* **2022**, *58*, 1545–1556.
24. Yan, M.Q.; Qian, H.; Yang, P.; Mao, W.M.; Jian, Q.W.; Jin, W.X. Analysis of micro-texture during secondary recrystallization in a Hi-B electrical steel. *J. Mater. Sci. Technol.* **2011**, *27*, 1065–1071. [CrossRef]
25. Hondros, E.D.; Stuart, E.H. Interfacial energies of textured silicon iron in the presence of oxygen. *Philos. Mag.* **1968**, *17*, 711–727. [CrossRef]